

# ***M*-subshell x-ray production cross sections of Au induced by highly charged F, C, and Li ions and protons: A large enhancement in the *M*<sub>3</sub> fluorescence yield**

Yeshpal Singh and Lokesh C. Tribedi\*

*Tata Institute of Fundamental Research, Homi Bhabha Road, Colaba, Mumbai 400 005, India*

(Received 27 August 2002; published 26 December 2002)

*M*-subshell x-ray production cross sections are measured for Au, induced by F ions in the energy range of 20 to 102 MeV. For a comparative study the measurements are also carried out for protons, He, Li, C ions at a few energies. We have derived the absolute cross sections for  $M\alpha\beta$  and  $M\gamma$  x rays as well as the total  $M$  x-ray cross sections. The intensity ratios,  $I(\gamma)/I(\alpha\beta)$ , of the  $M(\gamma)$  and  $M(\alpha\beta)$ , as well as the energy shifts of these lines signifying multiple vacancies in outer shells have also been studied as a function of projectile atomic number. The measured cross sections are compared with available theoretical calculations, namely, the ECPSSR based on the perturbed stationary state (PSS) approximation including the effects due to the increased binding energy, Coulomb deflection (C), energy loss (E), and relativistic (R) wave function. In case of the  $M\gamma$  the measured cross sections are much higher compared to the ECPSSR prediction which is attributed to a dramatic enhancement in the  $M_3$ -subshell fluorescence yield owing to multiple vacancies in  $N$  subshells. The enhancement strongly depends on the projectile atomic number.

DOI: 10.1103/PhysRevA.66.062709

PACS number(s): 34.50.Fa

## I. INTRODUCTION

The ionization of the inner atomic shells by highly charged particles is an important field of atomic collision physics from both the theoretical point of view and applications. For highly asymmetric collisions ( $Z_p/Z_t \ll 1$ ), where  $Z_p$  and  $Z_t$  are projectile and target atomic numbers, the direct Coulomb ionization mechanism is a dominating process [1–4]. Over the years a lot of work has been done on  $K$ - and  $L$ -shell ionization whereas very little is known regarding the  $M$ -shell processes. The studies on  $M$ -shell ionization provide more insight into the collision process since it possesses five subshells, giving rise to a much more complex system than  $K$  shell or even  $L$  shell which has only three subshells. To the best of our knowledge, there are very few experiments carried out on  $M$  x rays and most of them are confined to low  $Z$  projectiles like proton or alpha particles [5–13]. Only a few experiments [14–16] are carried out which use heavy ions as projectiles and thin foil targets. However, for the measurements with heavy ions, in which thick targets are used (i.e., about 30–40  $\mu\text{g}/\text{cm}^2$ ), the projectiles may exit with equilibrium charge states and the  $M$ -shell electron capture will also contribute substantially in the  $M$ -vacancy production. Therefore, for such thick targets, the x-ray yields cannot be taken as a measure of  $M$  ionization or transfer only. To overcome these problems one normally uses very thin targets (see [17] for a review) as has been done in Refs. [14–16] for  $M$  shell and Refs [18–21] for  $K$  shell. We have also measured the contribution in the  $M$ -shell x-ray yields due to  $M$ -shell (target) to  $K$ -shell (projectile) electron transfer by studying the charge state dependence of the x-ray yields. Using H-like and bare ions of F we found the x-ray intensity enhances substantially over that for low charge state (filled  $K$  shell for which no  $M$ - $K$  transfer is possible in thin targets) ions (see below). The x-ray yields obtained by using these low charge

state ions are essentially due to Coulomb ionization of the  $M$  shells.

It may be mentioned that the heavy ion induced ionization is more complicated since the process gets influenced due to the strong distortion of the initial target state by the highly charged ions. It has been shown that the so-called two-center effect and postcollision interactions strongly influence the electron angular distributions in ionization of outer-shell or loosely bound electrons in collisions with heavy projectiles. In case of inner-shell processes additional complications arise due to the multiple ionization in the outer shells which causes a substantial change in the x-ray fluorescence yields ( $\omega_i$ , for the  $i$ th subshell). In fact, it is demonstrated [22,23] that such enhancements are not necessarily of the same magnitude for all the subshells. For example,  $\omega_{L1}$ , for  $L_1$  subshells has been found to be dramatically enhanced in collisions with heavy ions whereas such enhancements in the  $\omega_{L2}$  or  $\omega_{L3}$  are not so high. It may also be noted that such enhancements, due to the interplay of Coster-Kronig transition strength and the radiative transition probabilities, are difficult to be predicted by the model calculations and therefore need to be measured especially in the presence of multiple outer-shell vacancies. However, it is required to have such investigations in case of  $M$ -subshell ionizations as well as the predictions on the subshell fluorescence yields. Here we present the measurement of the total  $M$  x ray,  $M\alpha\beta$  and  $M\gamma$  cross sections for Au in collisions with highly charged F ions as projectiles with energy ranging from 20 to 102 MeV. In order to make a comparative study of the subshell ionization and the fluorescence yield enhancement for different projectiles, we have also measured these quantities for proton, He, Li, and C ions at a few energies. The collision symmetry parameter  $S$  ( $=Z_p/Z_t$ ) is varied between 0.013 (for proton) and 0.114 (for F), signifying an asymmetric system. The average values of the reduced velocity  $v_p/v_e$  range from 0.45 to 1.03 for F ions. Here the  $v_p$  and  $v_e$  are the projectile and the  $M$ -shell electron average orbital velocity, respectively. The velocity range corresponds to the low to intermediate

\*Email address: lokesh@tifr.res.in

range in which the ionization process gets largely influenced by the increased binding energy as well the Coulomb deflection. Also the probabilities of various processes such as  $M$ -shell excitation,  $M$ -ionization, and  $M$ -shell electron transfer will have similar orders of magnitudes at the intermediate velocity range. Hence this regime provides a very good platform to provide a test to the theoretical models. The existing data on total  $M$  x-ray cross sections by Mehta *et al.* [14] on the similar collision systems cover a small energy range (less than 35 MeV). On the other hand, the present investigation spans on a wide range of energy (30–102 MeV) and we have measured absolute cross sections for  $M\alpha\beta$  as well as the  $M\gamma$  lines in addition to total cross sections. These studies therefore provide a crucial test for the various models of inner-shell ionization, e.g., the plane-wave Born approximation (PWBA) [3], the semiclassical approximation (SCA), and the perturbed stationary state (PSS) approach, including correction factors for projectile energy loss ( $E$ ), Coulomb deflection of the projectile ( $C$ ), and the relativistic motion ( $R$ ) of the orbital electrons (ECPSSR) [4].

It may be mentioned that the electron clouds in the  $M$  subshells can be strongly affected by the projectile ions which penetrate deeply inside to ionize the  $M$  subshells and as a result the various  $M$  subshells can be mixed with each other and may influence the ionization process. The effect of subshell couplings on the  $L$ -subshell ionization process has been studied [26,27] along with the investigation of the anisotropy in the  $L$  x-ray emission [28,29]. It is, however, shown that such coupling is important only in case of low energy (less than about 2 MeV/ $u$ ) [26] collisions.

## II. EXPERIMENTAL DETAILS

The experiment was performed with the 14 MV BARC-TIFR Pelletron accelerator at TIFR, Mumbai. Heavy ions of  $F^{4+}$  (20 MeV),  $F^{5+.7+.8+}$  (30 MeV),  $F^{6+.7+.8+.9+}$  (40 MeV),  $F^{6+.8+.9+}$  (57 MeV),  $F^{7+.8+.9+}$  (76 MeV),  $F^{7+}$  (85 MeV),  $F^{7+.8+.9+}$  (95 MeV), and  $F^{8+.9+}$  (102 MeV) were used for the measurement. In addition, protons (16 MeV),  $He^{++}$  (36 MeV),  $Li^{3+}$  (28 and 36 MeV), and C (48 MeV) ions were also used for a comparative study of the cross sections, peak energy shifts, and the intensity ratios. The mass and energy analyzed ion beams were made to fall on thin targets of Au ( $1.72 \mu\text{g}/\text{cm}^2$ ) on carbon backing (of thickness  $\sim 10 \mu\text{g}/\text{cm}^2$ ). While preparing the carbon-backed targets special care was taken for the purity of the carbon foil to minimize the background from low  $Z$  impurities in C foil (such as Ca) that overlaps the  $M$  x-ray spectrum. The targets were mounted at  $90^\circ$  to the beam direction on a rotatable multiple target holder assembly in an electrically isolated chamber. The vacuum inside the chamber during the experiment was  $\sim 10^{-6}$  Torr.

The x rays emitted from the target were detected by a Si(Li) detector with a  $25\text{-}\mu\text{m}$ -thick Be window and having 160-eV resolution at 5.9 keV. The intrinsic efficiency of the detector was measured using standard radioactive sources and PIXE (proton-induced x-ray emission) technique. The detector was mounted inside the vacuum chamber at angles  $55^\circ$  to the beam direction. The thickness of the targets were

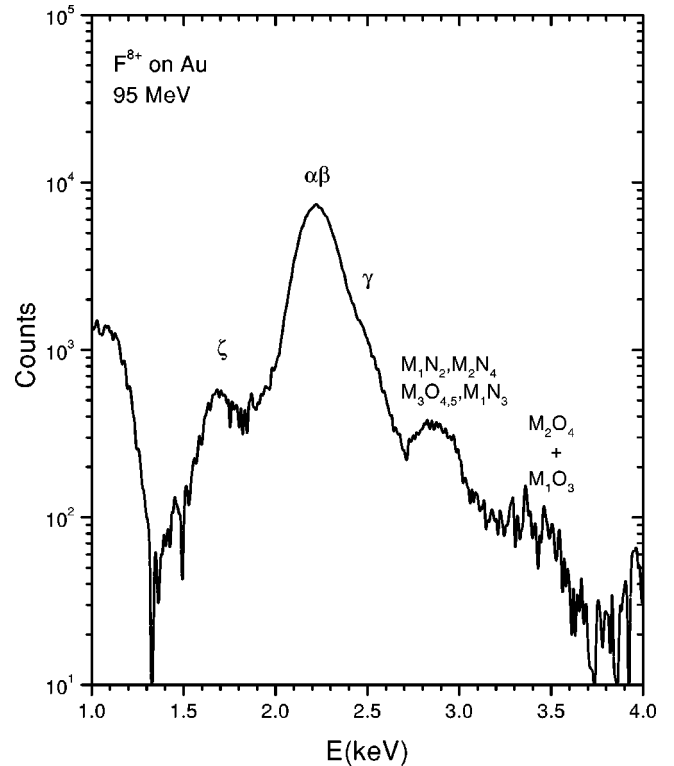


FIG. 1.  $M$  x-ray spectrum (background subtracted) of Au in collision with 95 MeV  $F^{8+}$ . The different components are indicated in the figure.

obtained, during the measurement, by counting Rutherford scattered particles at  $135^\circ$  and  $45^\circ$  to the beam direction using two surface barrier detectors. The total count rate under the x-ray spectrum was kept well below 500 counts/s in order to reduce the pile up. The beam current was measured from the entire chamber which was electrically isolated.

## III. DATA ANALYSIS

Typical  $M$  x-ray spectrum of Au is shown in Fig. 1 for 95 MeV F bombardment. As it is clear from the figure that the  $M$  x-ray spectra are quite complex, since some of the observed peaks represent several components of the  $M$  x-ray transitions which normally cannot be resolved by a Si(Li) detector. However, four different groups of lines are visible clearly, such as  $M\zeta$ ,  $M\alpha\beta$ ,  $M\gamma$ , and  $M_3O_{4,5} + M_1N_2$ . The  $M\alpha\beta$  line arises due to vacancy in the  $M_4/M_5$  subshells and  $M\gamma$  is due to the filling of the  $M_3$  vacancy ( $M_3N_5$  transition). The intensities of these lines therefore provide information regarding the probability of vacancy formation as well as the radiative transition or the subshell fluorescence yields. In Figs. 2(a)–2(e) we display the similar spectra obtained by different projectiles, such as  $p$ , He, Li, C, and F ions. The shift of the various lines are clearly visible compared to that for protons, as indicated by vertical lines which correspond to the  $M\alpha\beta$  peak for proton impact.

The peak areas in the x-ray spectra were estimated using a multi-Gaussian least-square-fitting program with the possibility of choosing variable width of the lines and background

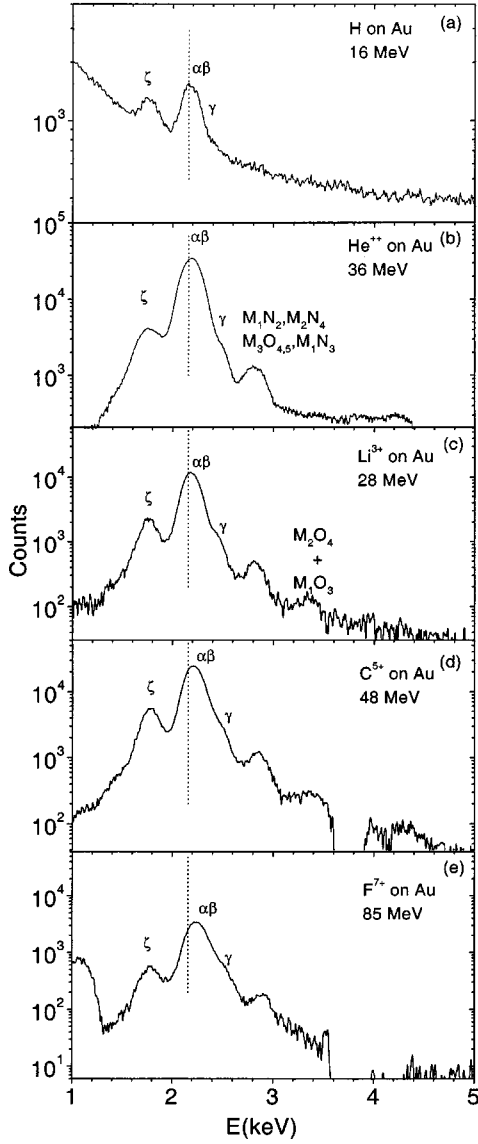


FIG. 2.  $M$  x-ray spectrum of Au in collision with (a) proton, (b)  $\text{He}^{++}$ , (c)  $\text{Li}^{3+}$ , (d)  $\text{C}^{5+}$ , and (e)  $\text{F}^{7+}$  with different beam energies as indicated. The vertical dotted line indicates the peak position under proton impact. The different components are indicated in the figure.

function. From the measured x-ray yields the x-ray production cross sections were estimated using the following relation:

$$\sigma_i^x = \frac{4\pi I_x \frac{d\sigma_R(\theta)}{d\Omega_p} \Delta\Omega_p}{\epsilon I_R \Delta\Omega_x}, \quad (1)$$

where  $\sigma_i^x$  is the x-ray production cross section of the  $i$ th line of the  $M$  x-ray spectrum,  $I_x$  being the measured x-ray count under the  $i$ th line. The quantity  $d\sigma_R(\theta)/d\Omega_p$  is the differential Rutherford scattering cross section,  $I_R$  is the particle count measured by surface barrier detector,  $\Delta\Omega_x$  is the solid angle subtended by the Si(Li) detector,  $\Delta\Omega_p$  is the solid angle subtended by the surface barrier detector, and  $\epsilon$  is the

TABLE I.  $M$  x-ray production cross sections ( $\sigma_{\alpha\beta}$ ,  $\sigma_\gamma$ , and  $\sigma_{total}$ ) due to  $M$ -subshell ionization of Au induced by F ions. Typical errors are about 15–20 %.

Target	Energy (MeV)	$\sigma_{\alpha\beta}$ (barn)	$\sigma_\gamma$ (barn)	$\sigma_{total}$ (barn)
Au	20	21400	3593	41975
	30	52200	12500	98210
	40	90500	11440	132250
	57	121000	17000	185150
	76	130000	20500	261050
	85	150000	26300	247250
	95	105000	20300	186990
	102	150000	22400	161000

intrinsic efficiency of the Si(Li). Equation (1) was used to calculate the x-ray production cross section only at low energies, i.e., below the Coulomb barrier, above which the normalization was done by measuring total beam current and target thickness.

The uncertainties in the measured cross sections in Table I were estimated to be about 15–20 % which include the errors due to counting statistics, background subtraction, detector solid angles, the target thickness (8%), and the efficiency of the Si(Li) detector (6–10 %).

The x-ray production cross sections for different  $M$  x-ray lines related to the ionization cross sections for different subshells  $\sigma_i^I$  ( $i=1,2,3,4,5$ ) of  $M$  shell in the following way:

$$\sigma_{M_1O_{23}}^x = \sigma_1^I \omega_1 \Gamma_{M_1O_{23}} / \Gamma_{M_1}, \quad (2)$$

$$\sigma_{M_2O_{14}}^x = [\sigma_1^I S_{12} + \sigma_2^I] \omega_2 \Gamma_{M_2O_{14}} / \Gamma_{M_2}, \quad (3)$$

$$\sigma_\gamma^x = [\sigma_1^I (S_{13} + S_{12}S_{23}) + \sigma_2^I S_{23} + \sigma_3^I] \omega_3 \Gamma_{M_\gamma} / \Gamma_{M_3}, \quad (4)$$

$$\begin{aligned} \sigma_\alpha^x = & [\sigma_1^I (S_{15} + S_{14}S_{45} + S_{13}S_{34}S_{45} + S_{13}S_{35} + S_{12}S_{23}S_{34}S_{45} \\ & + S_{12}S_{25} + S_{12}S_{23}S_{35} + S_{12}S_{24}S_{45}) + \sigma_2^I (S_{25} + S_{24}S_{45} \\ & + S_{23}S_{34}S_{45} + S_{23}S_{35}) + \sigma_3^I (S_{35} + S_{34}S_{45}) + \sigma_4^I S_{45} \\ & + \sigma_5^I] \omega_5 \Gamma_{M_\alpha} / \Gamma_{M_5}, \end{aligned} \quad (5)$$

$$\begin{aligned} \sigma_{\xi_1}^x = & [\sigma_1^I (S_{15} + S_{14}S_{45} + S_{13}S_{34}S_{45} + S_{13}S_{35} + S_{12}S_{23} + S_{34}S_{45} \\ & + S_{12}S_{25} + S_{12}S_{23}S_{35} + S_{12}S_{24}S_{45}) + \sigma_2^I (S_{25} + S_{24}S_{45} \\ & + S_{23}S_{34}S_{45} + S_{23}S_{35}) + \sigma_3^I (S_{35} + S_{34}S_{45}) + \sigma_4^I S_{45} \\ & + \sigma_5^I] \omega_5 \Gamma_{M_{\xi_1}} / \Gamma_{M_5}. \end{aligned} \quad (6)$$

Equations (2) to (6) link the experimentally measured line intensities to the five unknown subshell ionization cross section  $\sigma_i^I$  ( $i=1,2,3,4,5$ ), where  $S_{ij}$  are super-Coster-Kronig factors calculated by McGuire [24] and  $\Gamma_{M_i}$  are radiation widths for the  $i$ th subshell calculated by Bhalla [25].

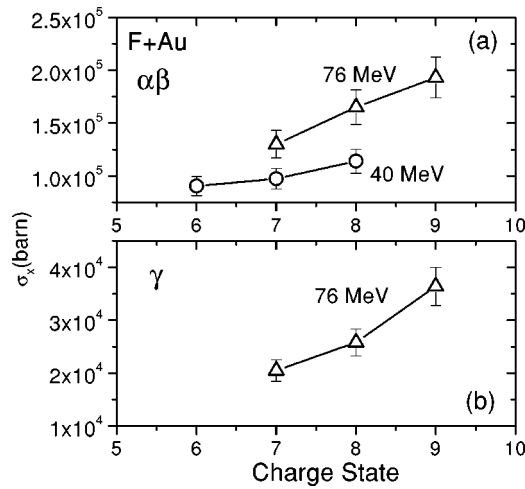


FIG. 3. Measured x-ray production cross sections of (a)  $M\alpha\beta$ , (b)  $M\gamma$  lines as a function of charge states, showing the contribution due to ionization (in the case of the lowest charge state) and  $M$ - $K$  electron transfer (for H-like ions). Data for two different beam energies are shown.

These above equations have been used to calculate theoretical x-ray cross sections for different lines. The required subshell resolved ionization cross sections were taken from ECPSSR calculations and then plotted against experimental cross sections.

#### IV. RESULTS AND DISCUSSIONS

##### A. $M$ -subshell ionization

Examples of the charge state dependence of the x-ray production cross sections are shown in Fig. 3, for two given beam energies. It may be seen that for H-like ions (and also for bare ions) there is an enhancement of the x-ray cross sections over that for the lowest charge state ions for which the  $K$  shells are filled. This is known to be due to the  $M$ - $K$  electron transfer which gives rise to additional  $M\alpha\beta$  (and also  $M\gamma$ ) x-ray yields. For the F ions the contribution in the  $M\alpha\beta$  yields due to the  $M$ - $K$  transfer is found to be about 25–30% of  $M$  ionization (see Fig. 3). In the rest of the paper we will discuss about the x-ray cross sections for the lowest charge states (i.e., with ions with filled  $K$  shells) which arise due to the  $M$  ionization only.

We show, in Fig. 4, the measured x-ray production cross sections for the  $M\alpha\beta$ ,  $M\gamma$ , and total  $M$  x ray as a function of the beam energy. The cross sections derived for low charge state ions, i.e., with no vacancies in the  $K$  shell, are taken as due to  $M$  ionization. The theoretical (ECPSSR) calculations are shown by solid continuous lines. It may be seen from Fig. 4(a) that the ECPSSR closely agrees with the  $M\alpha\beta$  cross sections for Au in the low-energy part and reproduces the data very well for the higher energies. The insets in the figures show the ratio of the experimental data to the ECPSSR predictions.

In case of  $M\gamma$  line, this deviation is very large, the theoretical cross sections being about a factor of eight lower compared to the data [Fig. 4(b)]. The total cross sections are

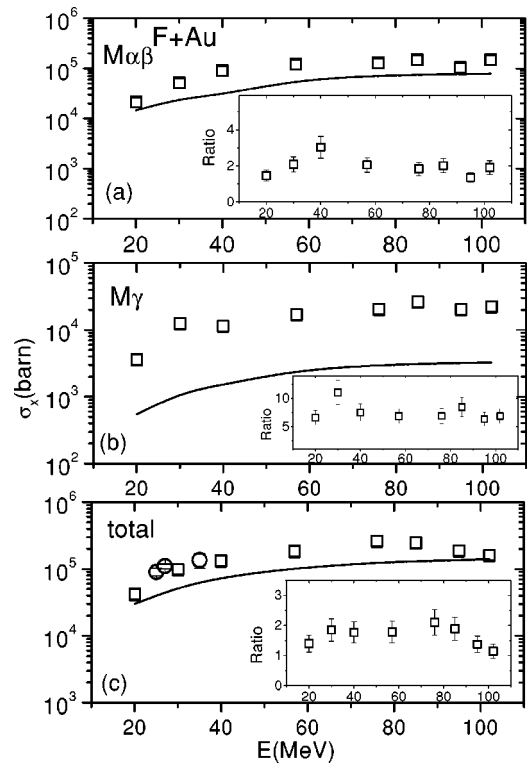


FIG. 4. Measured x-ray production cross sections of (a)  $M\alpha\beta$ , (b)  $M\gamma$  lines. The total  $M$  x-ray cross sections are shown in (c). The solid lines correspond to the ECPSSR predictions. The open circles in (c) are from Ref. [12]. The insets show the ratio of the data to the calculations.

shown in Fig. 4(c). The only existing total cross-section data for low-energy F ions [14] are also plotted [see the open circles in Figs. 4(c)]. It can be seen that the present experimental cross sections are in fairly good agreement with the earlier data sets. However, the calculated total cross sections fall below the experimental data by about 40–50% except at the highest energy and the discrepancy arises due the large disagreement in case of  $M\gamma$  cross sections.

The similar cross sections for the other light ion projectiles are shown in Figs. 5(a)–5(h). It can be seen that a good agreement is found between the  $M\alpha\beta$  data and the theory, only for protons [Fig. 5(a)]. In the case of  $\text{Li}^{3+}$  [Fig. 5(c)] and  $\text{C}^{5+}$  ions [Fig. 5(f)] the deviation increases and the calculations underestimate the  $M\alpha\beta$  cross sections. In case of  $M\gamma$  the deviation is larger compared to that for  $M\alpha\beta$  lines even for the proton beam [Fig. 5(b)]. These deviations are, however, even larger for the Li [Fig. 5(d)] and C [Fig. 5(g)] ions. The calculations, however, reproduce the total cross sections for Li ions [Fig. 5(e)] and underestimates to some extent for the C ions [Fig. 5(h)]. It may be noted that for H-like C ions there will be some contribution due to the  $M$ - $K$  transfer in the x-ray cross sections which will be small (estimated to be below about 10%) for  $M\alpha\beta$ . Therefore inclusion of the capture contribution in the calculations will reduce its difference with the measured data, but only by a small amount.

To investigate the large discrepancy in the case of  $M\gamma$  cross sections we have plotted, in Fig. 6, the intensity ratios

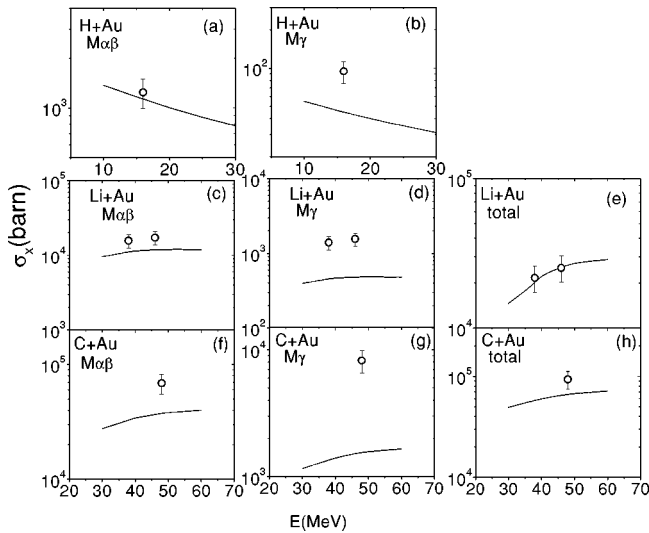


FIG. 5. Measured cross sections of  $M\alpha\beta$ ,  $M\gamma$  lines and the total  $M$  x rays for protons [(a) and (b)], for  $\text{Li}^{3+}$  [(c), (d), and (e)], and for  $\text{C}^{5+}$  ions [(f),(g),(h)]. The solid lines correspond to the ECPSSR predictions.

$I(\gamma)/I(\alpha\beta)$ . Figure 6 shows that this ratio varies between 0.15 to 0.24. A comparison with the ECPSSR is also made in this figure and the data fall much higher compared to the calculations. This ratio reflects the multiple vacancy in the outer shell as well as the vacancy probabilities in different  $M$  subshells. The ratio, as a function of  $Z_p$ , is plotted in Fig. 7. It is clearly seen that the deviation of the measured ratio from the ECPSSR prediction gradually increases with  $Z_p$  which shows the effect of multiple vacancy production for high  $Z_p$  projectiles. The ECPSSR does not reproduce the dependence of this ratio on  $Z_p$  and falls well below the experimental data, even for the lowest atomic number projectile. However, the deviation is caused partly due to multiple vacancies in outer shells and partly due to the inability of the

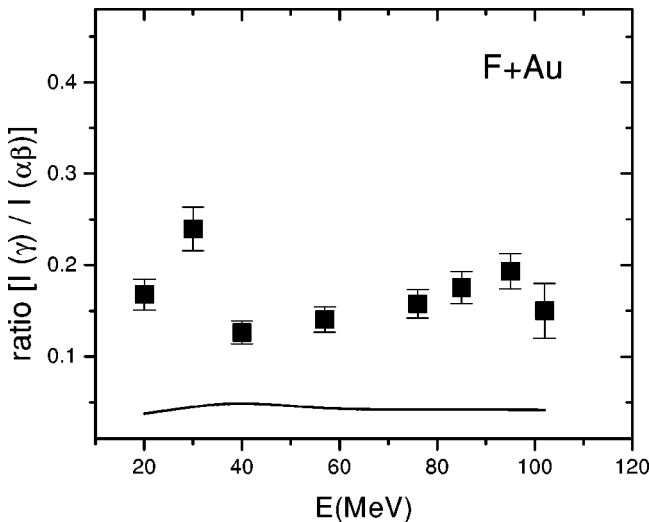


FIG. 6. The intensity ratios  $[I(\gamma)/I(\alpha\beta)]$  of the cross sections of  $M\alpha\beta$  and  $M\gamma$  lines for F-ion impact with different energies. The ECPSSR prediction is shown as a line.

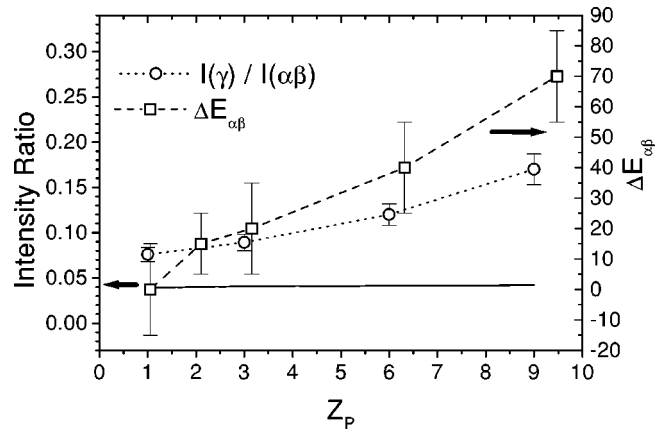


FIG. 7. The intensity ratios (left axis) of the  $M\gamma$  to the  $M\alpha\beta$  line, and the energy shifts of the  $M\alpha\beta$  line (right axis) as a function of  $Z_p$ . The ECPSSR prediction for the ratio is shown as a line.

theory to reproduce the  $M_3$  and  $M_{4,5}$  vacancy probability.

The energy shifts of the  $M\alpha\beta$  and  $M\gamma$  lines compared to their predicted positions, on the other hand, are purely caused due to the existence of the multiple vacancies in the outer shells at the time of x-ray emission. In case of Au, this shift is about  $67 \pm 10$  eV for  $M\alpha\beta$  lines ( $\Delta E_{\alpha\beta}$ ) and about the same for the  $M\gamma$  line. The shifts for He, Li, and C ions are found to be about 15, 20, and 36 eV, respectively, for  $M\alpha\beta$  lines. These shifts are found to increase sharply as a function of  $Z_p$  (also shown in Fig. 7). In fact,  $\Delta E_{\alpha\beta}$  increases more rapidly than the intensity ratio (in Fig. 7).

The shifts as well as the higher intensity ratios signify multiple vacancy production in the outer shells simultaneous with  $M$  vacancy of the target. This, in turn, results in the enhancement of the fluorescence yields. In particular, it is evident from the present data that the cross section for  $M\gamma$  (i.e.,  $M_3-N_5$ ), which arises from an  $M_3$  vacancy, is largely influenced by the multiple vacancy in outer shells and therefore the fluorescence yield for the  $M_3$  subshell is enhanced dramatically. This is due to the fact that due to multiple vacancies in the  $N$ -subshells some of the Coster-Kronig (CK) transitions cannot take place and therefore the radiative process dominates giving rise to higher x-ray cross sections compared to the theoretical predictions. This may be more clear from Table II in which we show the values of CK transition probabilities and the subshell fluorescence yields for Au. It may be worth noticing that the CK transition probability  $S_{35}$  (arising due to a vacancy in  $M_3$ ) is much higher (almost a factor of 200 large) compared to  $\omega_3$ . Therefore any multiple ionization in the  $N$  subshells (especially in  $N_5$ ) will reduce the  $S_{35}$  drastically since a particular CK channel (such as  $M_3-M_5N_5$ ) could be blocked giving a large  $\omega_3$ . In the case of the vacancy in the  $M_4$ , the  $\omega_4$  and the corresponding CK rate  $S_{45}$  have comparable values and therefore there is no drastic enhancement in the  $\omega_4$ . So no such large deviations are observed for the  $M\alpha\beta$ . A similar dramatic enhancement (by a factor of 2.5) in the  $L_1$ -subshell fluorescence yields for Yb and Au has been noticed in collisions with F ions due to the multiple vacancies and has been explained as an interplay between the CK rates and the  $\omega_1$  [22,23].

TABLE II. Atomic parameters related to  $M_3$  and  $M_4$  vacancy fillings used in the calculation (for Au), i.e., the CK rates and fluorescence yields.

$\omega_{M3}$	$S_{M3,4}$	$S_{M3,5}$	$\omega_{M4}$	$S_{M4,5}$	$\omega_{M5}$
$4.20 \times 10^{-3}$	0.114	0.782	0.0264	0.046	0.0256

The ratios of the experimentally measured x-ray cross sections ( $\sigma_{exp}$ ) of the  $M\gamma$  line to the ECPSSR predictions ( $\sigma_{ECPSSR}$ ) are shown in Fig. 8 as a function of  $Z_p$ . The similar ratios for the  $M\alpha\beta$  line are also shown in the same figure. The projectiles are having slightly different energies. However, since the ratios do not change appreciably in the present energy range, the projectiles with slightly different energies can be used to have a comparative study. In case of  $M\alpha\beta$  the ratio is very close to 1.0 for protons, implying a good agreement with the calculations. The deviation (from 1.0) for other projectiles are clearly seen to increase with  $Z_p$  and become a factor of about two for the F projectile. The ratio for the  $M\gamma$  line is, however, at least a factor of two higher compared to the expected value (i.e., one) even for the lowest  $Z_p$  projectile, a proton. The deviation increases rapidly as a function of  $Z_p$  from a value of two for a proton to about seven for an F projectile. One would have expected to have an approximately similar deviation from the theory for the  $M\alpha\beta$  and the  $M\gamma$  lines. Comparing the deviations (i.e., the ratios in Fig. 8) in the cases of the  $M\alpha\beta$  and  $M\gamma$  lines one may conclude from the additional deviation for  $M\gamma$  that the  $\omega_3$  could be enhanced by about a factor of 3.5 for F ions. These enhancement ( $\omega_3/\omega_3^0$ ) factors are about 2.0, 2.2, 3.0 for  $p$ , Li, and C ions and therefore increase strongly with the projectile atomic numbers. These estimates will provide very important input to calculate the effective fluorescence yields under heavy ion impact.

## V. CONCLUSIONS

We have measured the  $M$  x-ray (due to ionization) production cross sections for Au in collisions with highly charged F ions having energies between 20 and 102 MeV and other low atomic number projectiles, such as  $p$ , He, Li,

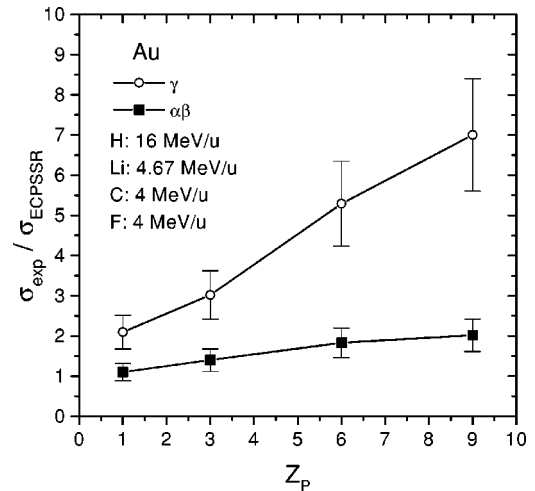


FIG. 8. The ratios of the experimental data to the ECPSSR predictions for the x-ray cross sections as a function of  $Z_p$ . The beam energies are indicated in the figure. The ratios are shown for both the  $M\alpha\beta$  and  $M\gamma$  lines. The dashed line corresponds to the expected ratio i.e., 1.0.

and C ions. Total cross sections as well as the cross sections of different  $M$  x-ray components, such as  $M\alpha\beta$  and  $M\gamma$  lines, are measured. In the case of the  $M\gamma$  the measured cross sections are much higher compared to the ECPSSR prediction, which is attributed to a dramatic enhancement in the  $M_3$  subshell fluorescence yield owing to multiple vacancies in  $N$  subshells. The deviations are much less for the  $M\alpha\beta$  cross sections. The measured energy shifts of the x-ray lines and the enhanced intensity ratios compared to the single hole value indicate a substantial multiple vacancies in the  $N$  subshells. A quantitative estimate of the enhancement in the  $\omega_3$  has been predicted as a function of projectile atomic numbers.

## ACKNOWLEDGMENTS

We would like to thank K. V. Thulasiram and D. Mitra for their help during the experiment and the machine staff for smooth running of the accelerator.

- 
- [1] W. Brandt, R. Laubert, and L. Sellin, *Phys. Rev.* **151**, 56 (1966).  
 [2] F.D. McDaniel, A. Toten, R.S. Petersen, J.L. Duggan, S.R. Wilton, J.D. Gressett, P.D. Miller, and G. Lapicki, *Phys. Rev. A* **19**, 1517 (1979).  
 [3] E. Merzbacher and H.W. Lewis, *Handbuch der Physik*, edited by S. Flugge (Springer-Verlag, Berlin, 1958, p. 166).  
 [4] W. Brandt and G. Lapicki, *Phys. Rev. A* **23**, 1717 (1981).  
 [5] Ch. Herren, B. Boschung, J.-Cl. Dousse, B. Galley, J. Hozowska, J. Kern, Ch. Rheme, M. Polasik, T. Ludziejewski, P. Rymuza, and Z. Sujkowski, *Phys. Rev. A* **57**, 235 (1998).  
 [6] K. Ishii, S. Morita, H. Tawara, H. Kaji, and T. Shiokawa, *Phys. Rev. A* **11**, 119 (1975).  
 [7] R. Mehta, J.L. Duggan, J.L. Price, F.D. McDaniel, and G. Lapicki, *Phys. Rev. A* **26**, 1883 (1982).  
 [8] M. Pajek, A.P. Kobzev, R. Sandrik, A.V. Skrypnik, R.A. Ilkhamov, S.H. Khusmurodov, and G. Lapicki, *Phys. Rev. A* **42**, 6582 (1990).  
 [9] M. Pajek, A.P. Kobzev, R. Sandrik, A.V. Skrypnik, R.A. Ilkhamov, S.H. Khusmurodov, and G. Lapicki, *Phys. Rev. A* **42**, 5298 (1990).  
 [10] R. Gowda and D. Powers, *Phys. Rev. A* **31**, 134 (1985).  
 [11] J.L. Price, J.L. Duggan, F.D. McDaniel, G. Lapicki, and R. Mehta, *Phys. Rev. A* **37**, 365 (1988).  
 [12] A. Amirabadi, H. Afarideh, S.M. Haji-saeid, F. Shokouhi, and H. Peyrovan, *J. Phys. B* **30**, 863 (1997).  
 [13] N.V. De Castro-Faria, F.L. Freire, Jr., A.G. de Pinho, and E.F. da Silveira, *Phys. Rev. A* **28**, 2770 (1983).

- [14] R. Mehta, J.L. Duggan, F.D. McDaniel, M.C. Andrews, G. Lapicki, P.D. Miller, L.A. Rayburn, and A.R. Zander, *Phys. Rev. A* **28**, 2722 (1983).
- [15] Y.C. Yu, H.L. Sun, J.L. Duggan, F.D. McDaniel, J.Y. Yin, and G. Lapicki, *Phys. Rev. A* **52**, 3836 (1995).
- [16] M.C. Andrews, F.D. McDaniel, J.L. Duggan, P.D. Miller, P.L. Pepmiller, H.F. Krause, T.M. Rosseel, L.A. Rayburn, R. Mehta, and G. Lapicki, *Phys. Rev. A* **36**, 3699 (1987).
- [17] T.J. Gray, in *Methods of Experimental Physics*, edited by P. Richard (Academic, New York, 1980), Vol. 17, p. 193.
- [18] J. Hall *et al.*, *Phys. Rev. A* **33**, 914 (1986); **28**, 99 (1983).
- [19] K. Wohrer, A. Chetioui, J.P. Rozet, A. Jolly, and C. Stephan, *J. Phys. B* **17**, 1575 (1984).
- [20] L.C. Tribedi, K.G. Prasad, P.N. Tandon, Z. Chen, and C.D. Lin, *Phys. Rev. A* **49**, 1015 (1994); L.C. Tribedi, K.G. Prasad, and P.N. Tandon, *ibid.* **47**, 3739 (1993).
- [21] J.A. Tanis, S.M. Shafroth, J.E. Willis, and J.R. Mowat, *Phys. Rev. Lett.* **45**, 1547 (1980).
- [22] W. Jitschin, R. Hippler, K. Finck, R. Schuch, and H.O. Lutz, *J. Phys. B* **16**, 4405 (1983), and references therein.
- [23] Y.P. Singh, D. Mitra, Lokesh C. Tribedi, and P.N. Tandon, *Phys. Rev. A* **63**, 012713 (2001).
- [24] E.J. McGuire, *Phys. Rev. A* **5**, 1043 (1972).
- [25] C.P. Bhalla, *J. Phys. B* **3**, 916 (1970).
- [26] L. Sarkadi and T. Mukoyama, *Phys. Rev. A* **37**, 4540 (1988).
- [27] L. Sarkadi, T. Mukoyama, and Z. Smit, *J. Phys. B* **29**, 2253 (1996).
- [28] W. Jitschin, R. Hippler, R. Shankar, H. Kleinpoppen, R. Schuch, and H.O. Lutz, *J. Phys. B* **16**, 1417 (1983).
- [29] J. Palinkas *et al.*, *J. Phys. B* **17**, 131 (1983).